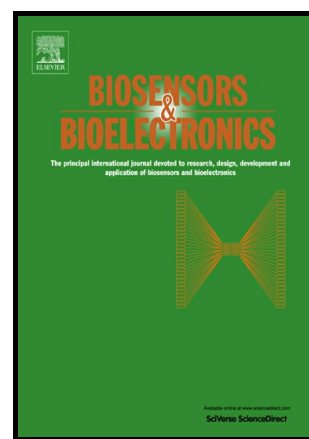


Author's Accepted Manuscript

A Unique Iridium(III) Complex-based Chemosensor for Multi-Signal Detection and Multi-Channel Imaging of Hypochlorous Acid in Liver Injury

Feiyue Zhang, Xiaowen Liang, Wenzhu Zhang, Yong-Lei Wang, Haolu Wang, Yousuf H. Mohammed, Bo Song, Run. Zhang, Jingli Yuan



PII: S0956-5663(16)30953-8
DOI: <http://dx.doi.org/10.1016/j.bios.2016.09.067>
Reference: BIOS9179

To appear in: *Biosensors and Bioelectronic*

Received date: 10 August 2016
Revised date: 9 September 2016
Accepted date: 19 September 2016

Cite this article as: Feiyue Zhang, Xiaowen Liang, Wenzhu Zhang, Yong-Lei Wang, Haolu Wang, Yousuf H. Mohammed, Bo Song, Run. Zhang and Jingli Yuan, A Unique Iridium(III) Complex-based Chemosensor for Multi-Signal Detection and Multi-Channel Imaging of Hypochlorous Acid in Liver Injury *Biosensors and Bioelectronic*, <http://dx.doi.org/10.1016/j.bios.2016.09.067>

This is a PDF file of an unedited manuscript that has been accepted for publication. As a service to our customers we are providing this early version of the manuscript. The manuscript will undergo copyediting, typesetting, and review of the resulting galley proof before it is published in its final citable form. Please note that during the production process errors may be discovered which could affect the content, and all legal disclaimers that apply to the journal pertain

A Unique Iridium(III) Complex-based Chemosensor for Multi-Signal Detection and Multi-Channel Imaging of Hypochlorous Acid in Liver Injury

Feiyue Zhang^a, Xiaowen Liang^b, Wenzhu Zhang^{a*}, Yong-Lei Wang^c, Haolu Wang^b, Yousuf H. Mohammed^b, Bo Song^a, Run Zhang^{d*}, Jingli Yuan^a

^aState Key Laboratory of Fine Chemicals, School of Chemistry, Dalian University of Technology, Dalian 116024, P. R China.

^bTherapeutics Research Centre, School of Medicine, The University of Queensland, Princess Alexandra Hospital, Woolloongabba, QLD 4102, Australia.

^cApplied Physical Chemistry, Department of Chemistry, KTH Royal Institute of Technology, SE-100 44 Stockholm, Sweden.

^dAustralian Institute for Bioengineering and Nanotechnology, The University of Queensland, St. Lucia, QLD 4072, Australia.

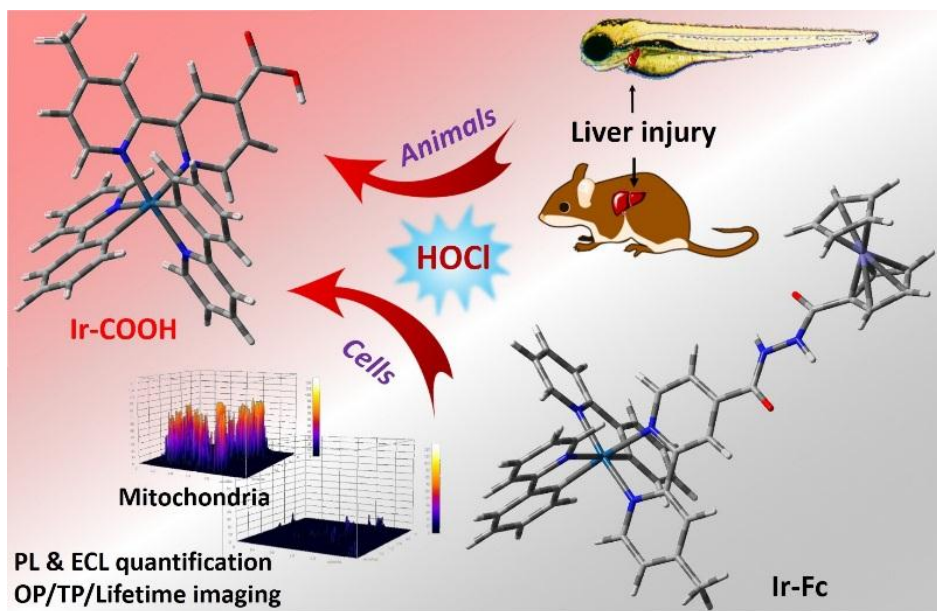
E-mail: wzhzhang@dlut.edu.cn

E-mail: r.zhang@uq.edu.au

ABSTRACT

Although hypochlorous acid (HOCl) has long been associated with a number of inflammatory diseases in mammalian bodies, the functions of HOCl in specific organs at abnormal conditions, such as liver injury, remain unclear due to its high reactivity and the lack of effective methods for its detection. Herein, a unique Ir(III) complex-based chemosensor, **Ir-Fc**, was developed for highly sensitive and selective detection of HOCl. **Ir-Fc** was designed by incorporating a ferrocene (Fc) quencher to a Ir(III) complex through a HOCl-responsive linker. In the presence of HOCl, the fast cleavage of Fc moiety in less than 1 second led to the enhancement of photoluminescence (PL) and electrochemical luminescence (ECL), by which the concentration of HOCl was determined by both PL and ECL analysis. Taking advantages of excellent properties of Ir(III) complexes, optical and electrochemical analyses of the response of **Ir-Fc** towards HOCl were fully investigated. Followed by the measurements of low cytotoxicity of **Ir-Fc** by MTT analysis, one-photon (OP), two-photon (TP) and lifetime imaging experiments were conducted to visualise the generation of HOCl in live microphage and HepG2 cells, and in zebrafish and mouse, respectively. Furthermore, the generation and distribution of HOCl in liver cells and liver injury of zebrafish and mouse were investigated. The results demonstrated the applicability of **Ir-Fc** as an effective chemosensor for imaging of HOCl generation in mitochondria of cells and liver injury *in vivo*, implying the potential of **Ir-Fc** for biomedical diagnosis and monitoring applications.

Graphic Abstract



A unique Ir(III) complex, **Ir-Fc**, was developed as a chemosensor for photoluminescence and electrochemical luminescence detection of HOCl with high sensitivity, specificity, and rapid optical response. The bioapplications of **Ir-Fc** were conducted in visualisation of endogenous HOCl generation in liver cells, and liver injury in zebrafish and mouse through one photon (OP), two photon (TP), and luminescence lifetime imaging.

KEYWORDS: Chemosensor, Iridium(III) complex, Bioimaging, Liver injury, Hypochlorous acid

1. INTRODUCTION

Hypochlorous acid (HOCl) is a strong oxidant that has potent antibacterial properties, playing important roles in the mammalian immune defence system (Dickinson and Chang 2011; Rongvaux et al. 2014; Winterbourn 2008). In animal and human bodies, the generation of HOCl is driven by a heme-containing enzyme, myeloperoxidase (MPO) catalysed oxidation reaction of chloride ion (Cl⁻) and hydrogen peroxide (H₂O₂) in activated leukocytes (Dickinson and Chang 2011; Lou et al. 2013; Sun et al. 2014; Xiao et al. 2015; Zhang et al. 2015b; Zhou et al. 2015). While endogenous generation of HOCl plays an important role in immune defence against microorganisms, it is also strongly associated with mediating tissues damage that has been recognised to cause or exacerbate a wide range of inflammatory diseases, such as lung, liver and kidney disease, atherosclerosis, neurodegenerative disorders, myocardial infarction, and cancer (Li et al. 2015; Wu et al. 2013; Xu et al. 2013; Zhang et al. 2015a; Zhu et al. 2014). Therefore, there has been an increasing interest in the investigation of generation, distribution, tissue concentration, and metabolism of HOCl in living organisms to understand its biological functions (Emrullahoglu et al. 2013; Xiao et al. 2015; Yang et al. 2011; Yuan et al. 2012; Zhao et al. 2016). It is well documented that HOCl is generated by neutrophils and diffuses into hepatocytes during hepatic injury (Iwamoto et al. 2002; Panizzi et al. 2009). Even so, in-situ detection of HOCl *in vivo*, particularly in a specific organ condition, remains a challenge due to its high reactivity (short lifetime, diffusion distance < 20 µm) with biological molecules and the existence of various antioxidants, such as glutathione (GSH), cysteine (Cys) in cells (Dickinson and Chang 2011; Meng et al. 2015; Winterbourn 2008; Yuan et al. 2015).

Over the past few years, a number of approaches have been developed to monitor the generation of HOCl in living systems, including colorimetric, luminescent/fluorescent,

electrochemical and chromatographic methods (Best et al. 2013; Goswami et al. 2015; Panizzi et al. 2009; Wu et al. 2013; Xiao et al. 2012; Xu et al. 2013; Yuan et al. 2015; Zhang et al. 2015a; Zhang et al. 2013a; Zhou et al. 2015; Zhu et al. 2014). Of these methods, luminescence/fluorescence detection of HOCl using small molecular probes is becoming increasingly attractive due to its inherent advantages such as high sensitivity and specificity, rapid analysis, and easy management (Guo et al. 2013; Hu et al. 2014; Hu et al. 2016; Zhang et al. 2013b; Zhang et al. 2016). Furthermore, employing microscopy molecular bioimaging technique, small molecular luminescence probes can be extensively applied to visualise the generation of HOCl *in-situ in vivo* (Cao et al. 2015; Kenmoku et al. 2007; Xiao et al. 2015). Accordingly, many molecular luminescence probes have recently been developed for the detection and imaging of HOCl in biological systems through exploring specific HOCl-mediated oxidation-reduction reactions (Xiao et al. 2012; Zhang et al. 2013b; Zhu et al. 2014).

Since each detection and imaging technology has its own consideration, molecular probes featuring multi-signal detection and multi-modal imaging are highly desirable to the design of chemosensors for HOCl detection in aqueous solutions and biological samples. This can be achieved by integrating HOCl-responsive groups with suitable luminophores, such as fluorescein, rhodamine, coumarin, cyanine, and metal complexes (Chen et al. 2016). Among various classes of luminophores, luminescent transition metal complexes, especially those of iridium(III) and ruthenium(II) complexes have attracted increasing interest in the development of responsive chemosensors and cell imaging probes due to their excellent photophysical, photochemical, and electrochemical properties (Chi et al. 2014; Coogan and Fernandez-Moreira 2014; Lo et al. 2012; Ma et al. 2012; Martin et al. 2014; Zhao et al. 2010).

In our previous works, several Ru(II) complex-based chemosensors for key biological markers, such as reactive oxygen/nitrogen species (ROS/RNS), amino acids and metal ions, have been developed and successfully applied to luminescent biosensing and bioimaging (Li et al. 2015; Zhang et al. 2010a; Zhang et al. 2012a; Zhang et al. 2010b). Multi-signal detection of these biomarkers through photoluminescence (PL) and electrogenerated chemiluminescence (ECL) has also been demonstrated by tuning emission properties of these complexes *via* different sensing mechanisms, such as photo-induced electron transfer (PET) (Li et al. 2015; Zhang et al. 2012a). Nevertheless, probes with multi-modal imaging of HOCl evolution in biological samples, especially in diseased models, have not been well developed. Moreover, imaging conducted by one-photon microscopy (OPM) requires a rather shorter excitation wavelength, which prevents their application in live tissue imaging because of the shortcomings of shallow penetration depth, and photo-damage to biological samples (Li et al. 2015; Liang et al. 2016; Yuan et al. 2015).

Cyclometalated Ir(III) complexes exhibit favourable photophysical properties (Coogan and Fernandez-Moreira 2014; Lo 2015; Ma et al. 2012; Ru et al. 2015; Zhao et al. 2010), including: i) high photostability, which enables real-time monitoring of targets without photobleaching; ii) large Stokes shift, which can minimise the possibility of self-quenching; iii) long luminescence lifetime, which allows them to be used for lifetime imaging and even time-gated luminescence imaging; iv) π -conjugated ligands, which endow them two-photon absorption behaviour, and to be used for two-photon (TP) bioimaging; v) abundant electrochemical properties, which suggest them being used in ECL detection; vi) low cytotoxicity, which provides them good application in biological samples. Therefore, these facts encourage us to engineer an Ir(III) complex-based

chemosensor for multi-signal detection of HOCl and multi-modal imaging of HOCl in biological systems.

Considering the effective triplet state quenching of ferrocene (Cao et al. 2015; Shu et al. 2012), and the excellent photophysical properties of cyclometalated Ir(III) complexes, in the present work, a unique Ir(III) complex-based chemosensor, **Ir-Fc**, was developed for rapid PL and ECL detection of HOCl. **Ir-Fc** was designed and synthesized by conjugation of ferrocene quencher and Ir(III) complex through a HOCl-sensitive hydrazine linker (Scheme 1). The produced chemosensor, **Ir-Fc**, is weakly luminescent in both PL and ECL analysis due to the presence of PET process. The specific cleavage of ferrocenyl quencher from the **Ir-Fc** mediated by HOCl led to the emission enhancement of the chemosensor, by which **Ir-Fc** was expected to be used for PL and ECL switch-ON sensing of HOCl. The cleavage of ferrocenyl by HOCl was then confirmed by the electrochemical test, including differential pulse voltammetry (DPV) and cyclic voltammograms (CVs) analysis. To demonstrate the broad bioapplications of **Ir-Fc**, HOCl generation in RAW 264.7 and HepG2 cells, and in livers of zebrafish and mouse was imaged by OPM, TPM and fluorescence lifetime imaging microscopy (FLIM). To the best of our knowledge, **Ir-Fc** is the first example of PL and ECL chemosensor for HOCl detection in injury cells and abnormal animal organs.

<Scheme 1 is here>

2. EXPERIMENTAL SECTION

2.1 Synthesis of Ir-Fc

A mixture of $[\text{Ir}(\text{ppy})_2\text{Cl}]_2$ (116 mg, 0.1 mmol) and ligand bpy-Fc (88 mg, 0.2 mmol) was suspended in 30 mL $\text{CH}_3\text{OH}/\text{CH}_2\text{Cl}_2$ (2:1, v/v) and heated at 60 °C under Ar atmosphere. After refluxing for 6 h with stirring, the solvent was evaporated under reduced pressure, and the crude product was purified by silica gel column chromatography with CH_2Cl_2 -MeOH as eluent. The product, **Ir-Fc**, was collected and isolated as its hexafluorophosphate salt. Yield: 70.2%. ESI-MS (m/z): 941.2. ^1H NMR (400 MHz, CD_3CN): δ 8.88 (s, 1H), 8.53 (s, 1H), 8.13 (d, $J = 5.7\text{Hz}$, 1H), 8.07 (d, $J = 8.4\text{Hz}$, 2H), 7.90-7.75 (m, 6H), 7.62 (dd, $J = 12.6, 5.3\text{Hz}$, 2H), 7.37 (d, $J = 5.4\text{Hz}$, 1H), 7.11-7.00 (m, 4H), 6.93 (tdd, $J = 7.4, 4.6, 1.2\text{Hz}$, 2H), 6.28 (dd, $J = 12.4, 7.3\text{Hz}$, 2H), 4.78 (s, 2H), 4.45 (s, 2H), 4.33 (s, 5H), 2.55 (s, 3H). ^{13}C NMR (126 MHz, CD_3CN): δ 169.49, 167.15, 162.92, 156.90, 154.51, 151.96, 151.25, 149.97-149.51, 148.99, 143.79, 141.66, 138.32, 131.26, 130.13, 129.20, 125.41, 124.63, 123.24, 122.64-121.76, 119.62, 116.98, 72.52, 70.79, 69.71, 68.13, 20.16. Elemental analysis calcd. (%) for $\text{C}_{45}\text{H}_{36}\text{F}_6\text{FeIrN}_6\text{O}_2\text{P}\cdot\text{H}_2\text{O}$: C 48.96, H 3.47, N 7.61; found (%): C 49.03, H 3.34, N 7.74.

2.2 Synthesis of Ir-COOH

A mixture of $[\text{Ir}(\text{ppy})_2\text{Cl}]_2$ (116 mg, 0.1 mmol) and bpy-COOH ligand (43 mg, 0.2 mmol) was suspended in 30 mL $\text{CH}_3\text{OH}/\text{CH}_2\text{Cl}_2$ (2:1, v/v) and heated at 65 °C under Ar atmosphere. After refluxing for 6 h with stirring, the solvent was evaporated under reduced pressure, and the crude product was purified by silica gel column chromatography with CH_2Cl_2 -MeOH as eluent. The product, **Ir-COOH**, was then collected and isolated as its hexafluorophosphate salt. Yield: 59.1%. ESI-HRMS (m/z): 715.1685, 737.1502 (M+Na). ^1H NMR (400 MHz, CD_3CN): δ 8.96 (s, 1H), 8.52 (s, 1H), 8.10-8.01 (m, 2H), 7.95 (d, $J = 5.5\text{ Hz}$, 1H), 7.89-7.85 (m, 1H), 7.85-7.75 (m, 5H), 7.60 (d, $J = 5.8\text{ Hz}$, 2H), 7.30 (d, $J = 5.7\text{ Hz}$, 1H), 7.06-6.97 (m, 4H), 6.91 (t, $J = 7.4\text{ Hz}$, 2H), 6.34-6.23 (m, 2H), 2.53 (s, 3H). ^{13}C NMR (126 MHz, CDCl_3): δ 168.09, 166.76, 156.12,

155.08, 151.66, 150.57, 150.15, 149.76, 148.43, 148.13, 143.43, 138.09, 131.76, 130.91, 128.65, 128.44, 125.25, 124.89, 124.53, 123.12, 122.70, 119.78, 119.62, 21.59.

3. RESULTS AND DISCUSSION

3.1 Synthesis and characterization of Ir-Fc for HOCl

As shown in Fig. S1, **Ir-Fc** was synthesized by a two-step reaction. Briefly, the synthesized ligand, bpy-Fc, was refluxed with $[\text{Ir}(\text{ppy})_2\text{Cl}]_2$ in $\text{CH}_3\text{OH}/\text{CH}_2\text{Cl}_2$ (v/v 2:1) for 6 h, the formed **Ir-Fc** was then purified by chromatography to give a 70.2% yield of **Ir-Fc**. **Ir-COOH** was synthesized and purified by a similar procedure. Structures of **Ir-Fc** and **Ir-COOH** were confirmed by NMR, MS (Fig. S2-S7), and elemental analysis. In addition, to verify the production of **Ir-COOH** after the reaction of **Ir-Fc** with HOCl, *in-situ* ESI-MS analysis was performed for the reaction solution. As shown in Fig. S8, the molecular-ion peak at m/z 715.3 was assigned to the $[\text{Ir}(\text{ppy})_2(\text{COOH-bpy})]^+$, indicating the successful cleavage of the ferrocenyl moiety quencher by HOCl and the generation of **Ir-COOH**.

As expected, **Ir-Fc** displayed weak emission due to the effective PET (Fig. S9), and the luminescence quantum yield (ϕ) was determined to be 0.0069. In the presence of HOCl, strong luminescence emission centered at 600 nm was observed with luminescence quantum yield (ϕ) of 0.11. The emission lifetime of **Ir-Fc** was determined to be 4.44 ns (Zhang et al. 2012b), while that of **Ir-COOH** was significantly increased to 90.52 ns. Such result in the changes of emission lifetime suggested that **Ir-Fc** could be used as a potential probing reagent for lifetime imaging of HOCl in biological systems. UV-Vis absorptions of **Ir-Fc** and **Ir-COOH** were also measured (Fig. S10). **Ir-Fc** showed strong absorption at 280-320 nm which can be assigned to the spin-allowed intraligand transition of ppy and the functionalized bpy ligand, while the absorption

bands in the visible region could be attributed to the overlap of the spin-allowed metal-to-ligand charge transfer (MLCT), ligand-to-ligand charge transfer (LLCT), and the d-d absorption band of ferrocene (around 460 nm).

3.2 PL response of Ir-Fc towards HOCl

As shown in Fig. 1A, **Ir-Fc** displayed weak and stable luminescent emission at 600 nm. Upon addition of HOCl, rapid luminescence enhancement was observed within 1 second, and then the luminescence intensity reached a steady level. The addition of another amount of HOCl induced similar enhancement in the luminescence intensity. These results suggest that **Ir-Fc** can truly serve as a chemosensor for rapid HOCl detection, which is one of the key requirements for a biosensor to be used in the monitoring of HOCl *in vivo*.

As shown in Fig. 1B, PL intensity of **Ir-Fc** was gradually increased upon the addition of HOCl, and the maximum PL intensity was observed in the presence of 20 equiv. of HOCl. By plotting the luminescence intensity against HOCl concentration, a linear correlation can be obtained in the range of 5-40 μM (Fig. 1C). The detection limit, calculated according to the method defined by IUPAC (Mocak 1997), is 93.3 nM, which indicates that **Ir-Fc** can be used as a sensitive chemosensor for the quantification of HOCl.

Specificity of PL response of **Ir-Fc** towards HOCl was examined, and the result was shown in Fig. 1D. No obvious PL enhancement was observed upon the additions of competitive ROS/RNS (including $\cdot\text{OH}$, H_2O_2 , O_2^- , $^1\text{O}_2$, ONOO^- , NO_3^- , NO_2^- , and NO) and biologically relevant metal ions (including Mg^{2+} , Fe^{2+} , Zn^{2+} , Fe^{3+} , Mn^{2+} , Na^+ , K^+ , Ni^{2+} , Cd^{2+} , Co^{2+} , Pb^{2+} and Cu^{2+}). In contrast, a remarkable enhancement in PL intensity was observed in the presence of HOCl, demonstrating the specific PL response of **Ir-Fc** towards HOCl. Such a specific PL

response enables **Ir-Fc** to be further useful as a luminescent chemosensor for imaging of HOCl in complicated biological samples.

<Fig. 1 is here>

The effect of pH on the PL response of **Ir-Fc** towards HOCl was determined. As shown in Fig. S13, in the absence of HOCl, the luminescence intensity of **Ir-Fc** was weak and stable in the range of pH 3-11. However, upon the addition of HOCl to the PBS solution containing **Ir-Fc**, PL intensities were remarkably increased. The slight decrease in luminescence intensities at acidic conditions could be attributed to the protonation of the carboxyl group of **Ir-COOH**. Since the dissociation of HOCl to hypochlorite anions (OCl^-) ($\text{pK}_a = 7.463$ at 35°C) (Zhang et al. 2013a), the HOCl-mediated oxidation reaction with hydrazine moiety could be partly blocked, which resulted in the diminishing of luminescence intensities at pH 8-11.

3.3 Electrochemical and ECL responses of **Ir-Fc** towards HOCl

As redox parameters critical to ECL, the cyclic voltammograms (CVs) of **Ir-Fc** and **Ir-COOH** were firstly characterized. As shown in Fig. S14, both complexes underwent irreversible oxidations. The CVs of **Ir-Fc** were characterized by 2 major electron oxidation peaks around $E_{1/2}^{\text{ox}} = 1.18$ V (vs Ag/AgCl) and $E_{1/2}^{\text{ox}} = 0.42$ V (vs Ag/AgCl), which could be assigned to the $\text{Ir}^{\text{III}}/\text{Ir}^{\text{IV}}$ and $\text{Fc}^0/\text{Fc}^{\text{I}}$ redox couples (Donato et al. 2013; Shu et al. 2012). Similar to **Ir-Fc**, a one-electron oxidation wave of $\text{Ir}^{\text{III}}/\text{Ir}^{\text{IV}}$ of **Ir-COOH** was determined to be $E_{1/2}^{\text{ox}} = 1.15$ V (vs Ag/AgCl). In addition, the onset potentials ($E_{\text{onset}}^{\text{ox}}$) of the $\text{Ir}^{\text{III}}/\text{Ir}^{\text{IV}}$ for **Ir-Fc** and **Ir-COOH** were also determined to be around 1.07 V and 1.05 V (vs Ag/AgCl), respectively. The close correspondence of the $E_{1/2}^{\text{ox}}$ for $\text{Ir}^{\text{III}}/\text{Ir}^{\text{IV}}$ of **Ir-Fc** and **Ir-COOH** suggested that the Ir^{III} centre was not greatly perturbed by the substitution of the bpy ligand of the complexes. Interestingly, it

was observed that the Fc^0/Fc^1 redox couple disappeared when **Ir-Fc** was transferred to **Ir-COOH**, indicating the cleavage of Fc moiety.

As shown in Fig. S15A, upon the addition of HOCl, the one-electron oxidation wave ($E_{1/2}^{\text{ox}}$) of Fc^0/Fc^1 redox couple was gradually weakened. The electrochemical response of **Ir-Fc** as a function of the added HOCl concentration was also examined by using the differential pulse voltammetry (DPV) measurement, by which a better-resolved potential information could be obtained. As shown in Fig. S15B, the one-electron oxidation peak of Fc^0/Fc^1 couple was obtained, accompanied by shoulder at 0.61 V (vs Ag/AgCl), which could be assigned to the redox potential of the ligand. In increasing amount of HOCl, the cleavage of the hydrazine moiety led to the diminishing of Fc^0/Fc^1 oxidation potential, and no DPV peak of Fc^0/Fc^1 couple was observed for **Ir-COOH**.

Although Ir(III) complexes have been extensively investigated in photophysics and photochemistry, their utilizations for ECL molecular sensing, especially for the multi-signal sensing combination of PL and ECL are rarely explored. As shown in Fig. S16, the ECL signal of **Ir-Fc** was extremely low, while **Ir-COOH**, the reaction product of **Ir-Fc** with HOCl, showed strong ECL emission. Most likely, the weak ECL of **Ir-Fc** can be attributed to the lack of ECL excited state of $^* \text{Ir}^{\text{III}}$ in the presence of ferrocenyl moiety, while the recovery of strong ECL of **Ir-COOH** is caused by the cleavage of ferrocenyl moiety in the Ir(III) complex (Lin et al. 2010). As shown in Fig. 2A, the ECL intensity of **Ir-Fc** was gradually increased upon the additions of different concentrations HOCl in PBS buffer containing 10 mM of TPrA. A good linearity was obtained in the range of 2.5-25 μM of HOCl concentration. The detection limit, calculated according to the method defined by IUPAC (Mocak 1997), is 0.28 μM . As shown in Fig. 2B,

strong ECL emission could only be observed when **Ir-Fc** was reacted with HOCl, corroborating the results of highly selective detection of HOCl.

<Fig. 2 is here>

3.4 Theoretical calculations

To further understand the photophysical properties, electron transition and the luminescence response of **Ir-Fc** in the presence of HOCl, density functional theory (DFT) and time-dependent DFT (TD-DFT) calculations were performed to estimate the corresponding transition energy of **Ir-Fc** and **Ir-COOH** based on the ground-state and excited-state geometries. Low-lying triplet excited states of **Ir-Fc** and **Ir-COOH** were then optimised by TD-DFT method to investigate the turn-ON luminescence changes, and the calculated data are shown in Fig. S21 and Table S3. Lowest-energy triplet excited state (T_1) of **Ir-COOH** was contributed from HOMO \rightarrow LUMO, which can be attributed to the emissions of $^3\text{MLCT}$ and $^3\text{LLCT}$, as has usually been demonstrated in the Ir(III) complexes (Ru et al. 2014; Sharma et al. 2014; Xiong et al. 2010). In contrast, the inefficient luminescence emission of **Ir-Fc** may be assigned to the $^3\text{ILCT}$, $^3\text{LMCT}$ and $^3\text{LLCT}$ based on HOMO-1 \rightarrow LUMO+7 and HOMO \rightarrow LUMO+9. These transitions may be attenuated by the electron transfer from Fc moiety to bpy ligand, leading to the luminescence quenching of **Ir-Fc** (Sharma et al. 2014). This feature of lack of excited state is in parallel with the electrochemical analysis for **Ir-Fc**. Therefore, the calculation data strongly supported the turn-ON luminescence of **Ir-Fc** upon interaction with HOCl.

The possibility of electron transfer process of **Ir-Fc** was then examined by the thermodynamic criteria, the free energy changes (ΔG_{PET}) of the PET effect, which was calculated using Rehm-Weller equation (Zhang et al. 2009). The free energy changes ΔG_{PET} was

determined to be $-23.335 \text{ kJ mol}^{-1}$ (-0.242 eV) by DFT calculation, and $-37.036 \text{ kJ mol}^{-1}$ (-0.384 eV) based on the measurement of absorption edge (Wang et al. 2012). Given that negative ΔG_{PET} represents the thermodynamical possibility of electron transfer, negative value of ΔG_{PET} obtained by both DFT calculation and experiments clearly demonstrated that electron transfer may occur for **Ir-Fc**.

3.5 Imaging of HOCl generation in biological systems

Prior to visualization of HOCl in living organisms, the cytotoxicity of **Ir-Fc** was evaluated on the basis of the reduction activity of methyl thiazolyltetrazolium (MTT) assay. In the current study, mouse microphage (RAW 264.7) and HepG2 cells were selected for the cytotoxicity evaluation. As shown in Fig. S22, the cell viabilities are all greater than 90% after exposure of $150 \mu\text{M}$ of **Ir-Fc** for 24 h, suggesting that the **Ir-Fc** has good biocompatibility.

Increased generation of reactive oxygen species (ROS), including HOCl, has long been observed in cancer cells, while the HOCl generation during cancer chemotherapy is less clear (Trachootham et al. 2009). Thus, we next investigated the HOCl generation in HepG2 cells upon treatment with anticancer drug, elesclomol. As shown in Fig. 3, **Ir-Fc**-loaded HepG2 cells exhibited almost no luminescence, while the intracellular luminescence was significantly increased when the cells were further incubated with elesclomol. These results suggested that the endogenous HOCl generation in HepG2 cells during chemotherapy could be detected by employing **Ir-Fc** as a sensing probe.

<Fig. 3 is here>

It was noticed that the intracellular luminescence of **Ir-Fc**-loaded HepG2 cells was presented partly in the cytoplasm (Fig. 3F). This observation attracted our attention to investigate the subcellular localization of **Ir-Fc** in HepG2 cells using laser-scanning confocal microscopy. Since it has been known that Ir(III) complexes can cross the membrane to be accumulated in the mitochondria (Chen et al. 2014; Sun et al. 2016), co-localization experiments of **Ir-Fc** and mitochondria were carried out for HepG2 cells. As shown in Fig. S24 and S25, red luminescence of **Ir-Fc** was significantly co-localized with the green luminescence of MitoTracker green, confirming that **Ir-Fc** molecules were distributed in mitochondria of cancer cells. The intensity correlation quotients (ICQ) for two stains was determined to be 0.392, which is close to 0.5, suggesting that the stains of **Ir-Fc** and MitoTracker green are dependent. Both the Pearson's correlation coefficient (0.884) and the Mander's overlap coefficient (0.892) are close to 1, indicating the mitochondria distribution of red luminescence of **Ir-Fc** in HepG2 cells.

Ir-Fc was then applied to visualize endogenous HOCl production during drug stimulation in live zebrafish. In a control group, Zebrafish showed almost non-luminescence upon incubation with **Ir-Fc** alone for 2 h (Fig. S27). In contrast, as shown in Fig. 4, bright red luminescence was observed when zebrafish was stimulated with LPS and treated with **Ir-Fc** for 2 h, respectively. Importantly, it was noticed that the luminescence mainly localized in the liver of zebrafish, suggesting the endogenous HOCl generation in liver tissue (Li et al. 2015). It is well known that LPS can cause liver injury as an endotoxin, as the consequence, the increase of HOCl generation induced by the endotoxic shock can be confirmed by employing **Ir-Fc** as a HOCl sensing probe (Li et al. 2015).

<Fig. 4 is here>

Next, we demonstrated the two-photon (TP) imaging of HOCl generation induced by ischemia-reperfusion (I/R) injury in fresh mouse liver tissue. Mouse hepatic artery was clamped by using a microvascular clamp for 0.5 h, followed by reperfusion in the liver for 2 h. As shown in Fig. 5, a significant increase in red emission was observed in hepatocytes with decreased autofluorescence in I/R liver. The enhancement of luminescence intensity is due to the HOCl generation during hepatic I/R injury, which has been well documented. The result indicated the feasibility of detection of HOCl generation in living liver tissue by utilizing **Ir-Fc** as a TP imaging probe.

<Fig. 5 is here>

The increase of luminescence lifetime upon detection of HOCl promoted us to map the changes of lifetime by lifetime imaging in fresh liver tissues. The luminescence lifetime of **Ir-Fc** in normal liver tissue was measured as ca. 1.9 ns, while it was significantly increased to 65.6 ns in I/R injury liver (Fig. S28, S29). In consistence with the result of lifetime measurement in buffer solution, the increase in luminescence lifetime could be attributed to the formation of **Ir-COOH**, the reaction product of **Ir-Fc** with HOCl in the I/R injury liver. In addition, it was noticed that the luminescence lifetime of **Ir-Fc** in liver showed 2.5 ns shorter than that in buffer solution, which might be due to the effects of solvents and surroundings of the sensor molecules.

4. CONCLUSIONS

In the present work, a unique Ir(III) complex, **Ir-Fc**, was designed and synthesized for the detection of HOCl in aqueous and biological media. **Ir-Fc** showed almost non-luminescence in both PL and ECL due to the presence of effective PET process, while its emission was remarkably enhanced by a HOCl-mediated cleavage reaction, by such a mechanism the

quantification of HOCl could be achieved. The results of optical and electrochemical measurements indicated that **Ir-Fc** could be used as a multi-signal chemosensor for highly sensitive and selective detection of HOCl in less than 1 second. The cell experimental results revealed that **Ir-Fc** was low cytotoxic, and could be used as a luminescent sensing probe for imaging of HOCl in biological samples. Further experiments on visualisation of HOCl in livers of zebrafish and mouse demonstrated that **Ir-Fc** was suitable to be used for monitoring of HOCl generation in liver injury. The advances of the present HOCl chemosensor could not only highlight the application value of luminescence metal complexes in biosensing and bioimaging, but also could open a new field for the application of chemosensors in disease diagnosis and monitoring. It is also believed that the successful applications of **Ir-Fc** for HOCl sensing and bioimaging have the potential to advance the fields of current analytical science and biomedicine.

Acknowledgments

This work was financially supported by the National Natural Science Foundation of China (No. 21475015 and No. 21275025).

References

- Best, Q.A., Sattenapally, N., Dyer, D.J., Scott, C.N., McCarroll, M.E., 2013. *J. Am. Chem. Soc.* 135, 13365-13370.
- Cao, L., Zhang, R., Zhang, W., Du, Z., Liu, C., Ye, Z., Song, B., Yuan, J., 2015. *Biomaterials* 68, 21-31.
- Chen, X., Wang, F., Hyun, J.Y., Wei, T., Qiang, J., Ren, X., Shin, I., Yoon, J., 2016. *Chem. Soc. Rev.* 45, 2976-3016.
- Chen, Y., Qiao, L., Ji, L., Chao, H., 2014. *Biomaterials* 35, 2-13.

- Chi, Y., Tong, B., Chou, P.-T., 2014. *Coord. Chem. Rev.* 281, 1-25.
- Coogan, M.P., Fernandez-Moreira, V., 2014. *Chem. Commun.* 50, 384-399.
- Dickinson, B.C., Chang, C.J., 2011. *Nat. Chem. Bio.* 7, 504-511.
- Donato, L., McCusker, C.E., Castellano, F.N., Zysman-Colman, E., 2013. *Inorg. Chem.* 52, 8495-8504.
- Emrullahoglu, M., Ucuncu, M., Karakus, E., 2013. *Chem. Commun.* 49, 7836-7838.
- Goswami, S., Aich, K., Das, S., Pakhira, B., Ghoshal, K., Quah, C.K., Bhattacharyya, M., Fun, H.-K., Sarkar, S., 2015. *Chem. Asian. J.* 10, 694-700.
- Guo, T., Cui, L., Shen, J., Wang, R., Zhu, W., Xu, Y., Qian, X., 2013. *Chem. Commun.* 49, 1862-1864.
- Hu, J.J., Wong, N.-K., Gu, Q., Bai, X., Ye, S., Yang, D., 2014. *Org. Lett.* 16, 3544-3547.
- Hu, J.J., Wong, N.-K., Lu, M.-Y., Chen, X., Ye, S., Zhao, A.Q., Gao, P., Yi-Tsun Kao, R., Shen, J., Yang, D., 2016. *Chem. Sci.* 7, 2094-2099.
- Iwamoto, A., Egashira, T., Takayama, F., Yamanaka, Y., Noguchi, T., 2002. *Pathophysiology : the official journal of the International Society for Pathophysiology / ISP* 8(3), 167-174.
- Kenmoku, S., Urano, Y., Kojima, H., Nagano, T., 2007. *J. Am. Chem. Soc.* 129, 7313-7318.
- Li, G., Lin, Q., Sun, L., Feng, C., Zhang, P., Yu, B., Chen, Y., Wen, Y., Wang, H., Ji, L., Chao, H., 2015. *Biomaterials* 53, 285-295.
- Liang, X., Wang, H., Zhu, Y., Zhang, R., Cogger, V.C., Liu, X., Xu, Z.P., Grice, J.E., Roberts, M.S., 2016. *ACS nano.* 10, 387-395.
- Lin, H., Cinar, M. E., Schmittel, M., 2010. *Dalton Trans.* 39, 5130-5138
- Lo, K.K.-W., 2015. *Acc. Chem. Res.* 48, 2985-2995.
- Lo, K.K.-W., Choi, A.W.-T., Law, W.H.-T., 2012. *Dalton Trans.* 41, 6021-6047.

- Lou, Z., Li, P., Pan, Q., Han, K., 2013. *Chem. Commun.* 49, 2445-2447.
- Ma, D.-L., Ma, V.P.-Y., Chan, D.S.-H., Leung, K.-H., He, H.-Z., Leung, C.-H., 2012. *Coord. Chem. Rev.* 256, 3087-3113.
- Martin, A., Byrne, A., Burke, C.S., Forster, R.J., Keyes, T.E., 2014. *J. Am. Chem. Soc.* 136, 15300-15309.
- Meng, Q., Jia, H., Succar, P., Zhao, L., Zhang, R., Duan, C., Zhang, Z., 2015. *Biosens. Bioelectron.* 74, 461-468.
- Mocak, J., 1997. *Pure.Appl.Chem.* 69, 297-328.
- Panizzi, P., Nahrendorf, M., Wildgruber, M., Waterman, P., Figueiredo, J.-L., Aikawa, E., McCarthy, J., Weissleder, R., Hilderbrand, S.A., 2009. *J. Am. Chem. Soc.* 131, 15739-15744.
- Rongvaux, A., Willinger, T., Martinek, J., Strowig, T., Gearty, S.V., Teichmann, L.L., Saito, Y., Marches, F., Halene, S., Palucka, A.K., Manz, M.G., Flavell, R.A., 2014. *Nat. Biotech.* 32, 364-372.
- Ru, J.-X., Guan, L.-P., Tang, X.-L., Dou, W., Yao, X., Chen, W.-M., Liu, Y.-M., Zhang, G.-L., Liu, W.-S., Meng, Y., Wang, C.-M., 2014. *Inorg. Chem.* 53, 11498-11506.
- Ru, J., Tang, X., Ju, Z., Zhang, G., Dou, W., Mi, X., Wang, C., Liu, W., 2015. *ACS Appl. Mater.Interfaces* 7, 4247-4256.
- Sharma, S., Kim, H., Lee, Y.H., Kim, T., Lee, Y.S., Lee, M.H., 2014. *Inorg. Chem.* 53, 8672-8680.
- Shu, Q., Birlenbach, L., Schmittel, M., 2012. *Inorg. Chem.* 51, 13123-13127.
- Sun, L., Chen, Y., Kuang, S., Li, G., Guan, R., Liu, J., Ji, L., Chao, H., 2016. *Chem. Eur. J.* 22, 8955-8965.

- Sun, M., Yu, H., Zhu, H., Ma, F., Zhang, S., Huang, D., Wang, S., 2014. *Anal. Chem.* 86, 671-677.
- Trachootham, D., Alexandre, J., Huang, P., 2009. *Nat. Rev. Drug. Discov.* 8, 579-591.
- Wang, R., Liu, D., Zhang, R., Deng, L., Li, J., 2012. *J. Mater. Chem.* 22, 1411-1417.
- Winterbourn, C.C., 2008. *Nat. Chem. Biol.* 4, 278-286.
- Wu, X., Li, Z., Yang, L., Han, J., Han, S., 2013. *Chem. Sci.* 4, 460-467.
- Xiao, H., Xin, K., Dou, H., Yin, G., Quan, Y., Wang, R., 2015. *Chem. Commun.* 51, 1442-1445.
- Xiao, Y., Zhang, R., Ye, Z., Dai, Z., An, H., Yuan, J., 2012. *Anal. Chem.* 84, 10785-10792.
- Xiong, L., Zhao, Q., Chen, H., Wu, Y., Dong, Z., Zhou, Z., Li, F., 2010. *Inorg. Chem.* 49, 6402-6408.
- Xu, Q., Lee, K.-A., Lee, S., Lee, K.M., Lee, W.-J., Yoon, J., 2013. *J. Am. Chem. Soc.* 135, 9944-9949.
- Yang, Y.-C., Lu, H.-H., Wang, W.-T., Liao, I., 2011. *Anal. Chem.* 83, 8267-8272.
- Yuan, L., Lin, W., Xie, Y., Chen, B., Song, J., 2012. *Chem. Eur. J.* 18, 2700-2706.
- Yuan, L., Wang, L., Agrawalla, B.K., Park, S.-J., Zhu, H., Sivaraman, B., Peng, J., Xu, Q.-H., Chang, Y.-T., 2015. *J. Am. Chem. Soc.* 137, 5930-5938.
- Zhang, K.Y., Zhang, J., Liu, Y., Liu, S., Zhang, P., Zhao, Q., Tang, Y., Huang, W., 2015. *Chem. Sci.* 6, 301-307.
- Zhang, R., Song, B., Dai, Z., Ye, Z., Xiao, Y., Liu, Y., Yuan, J., 2013a. *Biosens. Bioelectron.* 50, 1-7.
- Zhang, R., Ye, Z., Song, B., Dai, Z., An, X., Yuan, J., 2013. *Inorg. Chem.* 52, 10325-10331.
- Zhang, R., Ye, Z., Wang, G., Zhang, W., Yuan, J., 2010. *Chem. Eur. J.* 16, 6884-6891.

- Zhang, R., Ye, Z., Yin, Y., Wang, G., Jin, D., Yuan, J., Piper, J.A., 2012a. *Bioconjugate Chem.* 23, 725-733.
- Zhang, R., Yu, X., Ye, Z., Wang, G., Zhang, W., Yuan, J., 2010. *Inorg.Chem.* 49, 7898-7903.
- Zhang, R., Zhao, J., Han, G., Liu, Z., Liu, C., Zhang, C., Liu, B., Jiang, C., Liu, R., Zhao, T., Han, M.-Y., Zhang, Z., 2016. *J. Am. Chem. Soc.* 138, 3769-3778.
- Zhang, W., Liu, W., Li, P., kang, J., Wang, J., Wang, H., Tang, B., 2015. *Chem. Commun.* 51, 10150-10153.
- Zhang, W., Zhang, R., Zhang, J., Ye, Z., Jin, D., Yuan, J., 2012b. *Anal. Chim. Acta* 740, 80-87.
- Zhang, X., Chi, L., Ji, S., Wu, Y., Song, P., Han, K., Guo, H., James, T.D., Zhao, J., 2009. *J. Am. Chem. Soc.* 131, 17452-17463.
- Zhao, C., An, J., Zhou, L., Fei, Q., Wang, F., Tan, J., Shi, B., Wang, R., Guo, Z., Zhu, W.-H., 2016. *Chem. Commun.* 52, 2075-2078.
- Zhao, Q., Li, F., Huang, C., 2010. *Chem. Soc. Rev.* 39, 3007-3030.
- Zhou, J., Li, L., Shi, W., Gao, X., Li, X., Ma, H., 2015. *Chem. Sci.* 6, 4884-4888.
- Zhu, H., Fan, J., Wang, J., Mu, H., Peng, X., 2014. *J. Am. Chem. Soc.* 136, 12820-12823.

Scheme 1. Design of the luminescent chemosensor, **Ir-Fc**, for selective and sensitive detection of HOCl.

Fig. 1. PL response of **Ir-Fc** towards HOCl. (A) Time course of the luminescence response of **Ir-Fc** (10 μM) towards HOCl addition (final concentration of 7.5 μM for each). (B) Excitation and emission spectra of **Ir-Fc** (10 μM) in the presence of various concentrations of HOCl (0, 5, 10, 15, 20, 25, 30, 40, 60, 80, 100, 150 and 200 μM). (C) Calibration curve for HOCl detection using **Ir-Fc** (10 μM) as a sensing probe. (D) PL intensities of **Ir-Fc** (10 μM) in the presence of different bioactive species (100 μM). (a) blank, (b) HOCl, (c) $\cdot\text{OH}$, (d) H_2O_2 , (e) O_2^- , (f) $^1\text{O}_2$, (g) ONOO^- , (h) NO_2^- , (i) NO_3^- , (j) NO, (k) Fe^{2+} , (l) metal ions (100 μM for each, including Mg^{2+} , Zn^{2+} , Fe^{3+} , Mn^{2+} , Na^+ , K^+ , Ni^{2+} , Cd^{2+} , Co^{2+} , Pb^{2+} and Cu^{2+}).

Fig. 2. (A) ECL responses of **Ir-Fc** (10 μM) towards various concentrations of HOCl (0, 2, 5, 10, 15, 20, and 25 μM) in 25 mM PBS-EtOH (1:1, v/v) buffer of pH 7.4 containing 10 mM TPrA (the inset shows the calibration curve for the ECL detection of HOCl). Scan rate of ECL was 0.15 V/s. (B) ECL intensities of **Ir-Fc** (10 μM) in the presence of different bioactive species (100 μM). (a) blank, (b) HOCl, (c) $\cdot\text{OH}$, (d) H_2O_2 , (e) O_2^- , (f) $^1\text{O}_2$, (g) ONOO^- , (h) NO_2^- , (i) NO_3^- , (j) NO, (k) Fe^{2+} , (l) metal ions (including Mg^{2+} , Zn^{2+} , Fe^{3+} , Mn^{2+} , Na^+ , K^+ , Ni^{2+} , Cd^{2+} , Co^{2+} , Pb^{2+} and Cu^{2+}).

Fig. 3. Confocal luminescence imaging of HOCl generation in HepG2 cells during chemotherapy. (A) and (E) Bright-field images of HepG2 cells before and after treatment with elesclomol. (B) Luminescence image of the **Ir-Fc**-loaded cells. (F) Luminescence image of the **Ir-Fc**-loaded cells that were further treated with elesclomol for another 3 h. (C) and (G) Image J

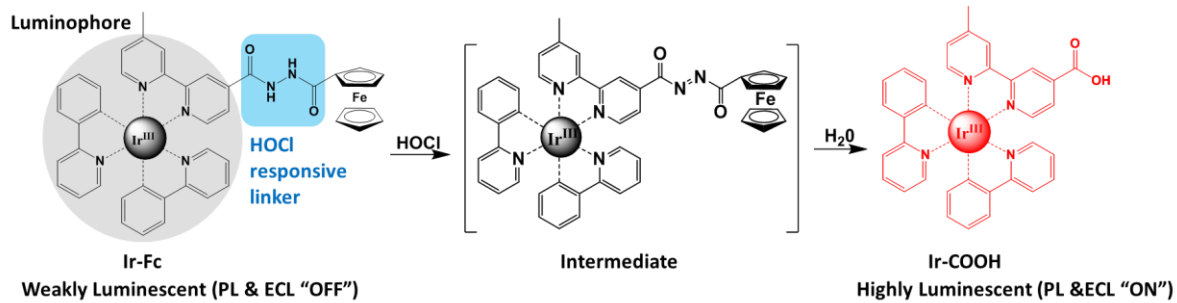
3-D interactive intensity analysis of luminescence images of (B) and (F). (D) and (H) Merged images of (B) and (F) with their bright-field images. Scale bar: 10 μm .

Fig. 4. Bright-field (A), luminescence (B) and merged (C) images of LPS (2 $\mu\text{g}/\text{mL}$) pre-treated zebrafish incubated with 100 μM **Ir-Fc** for 2 h.

Fig. 5. Detection of ischemia-reperfusion (I/R) injury-induced HOCl production using **Ir-Fc** as a TP sensing probe in mouse liver under TP microscope. Scale bar: 40 μm .

Accepted manuscript

Scheme 1.



Accepted manuscript

Fig. 1.

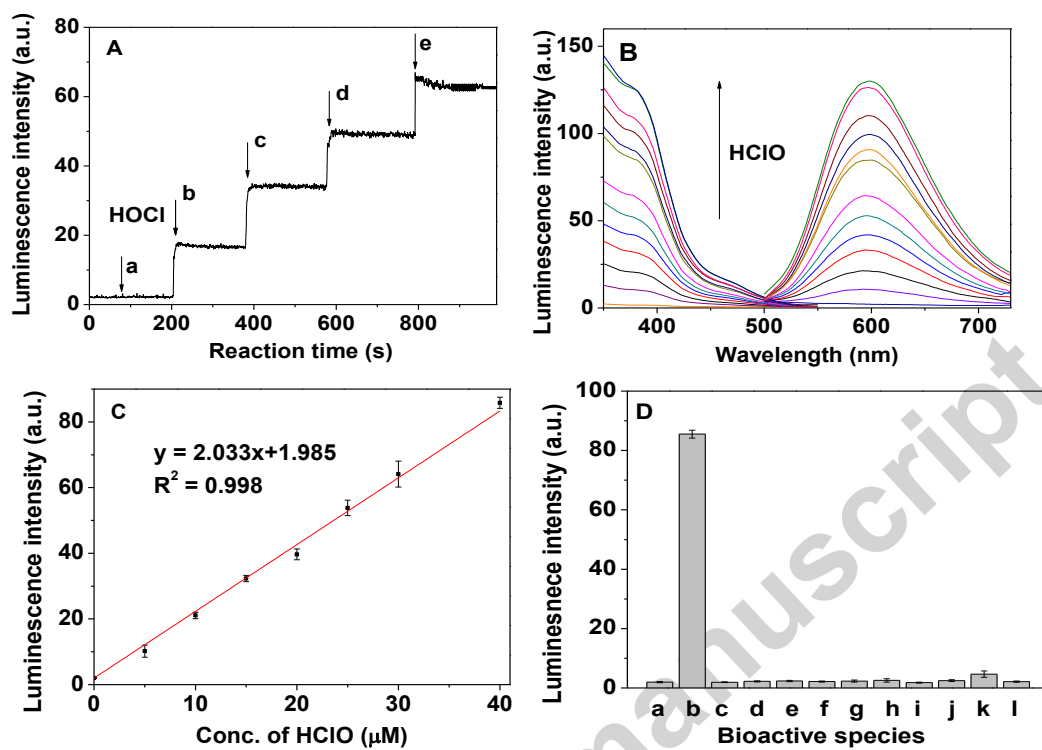


Fig. 2

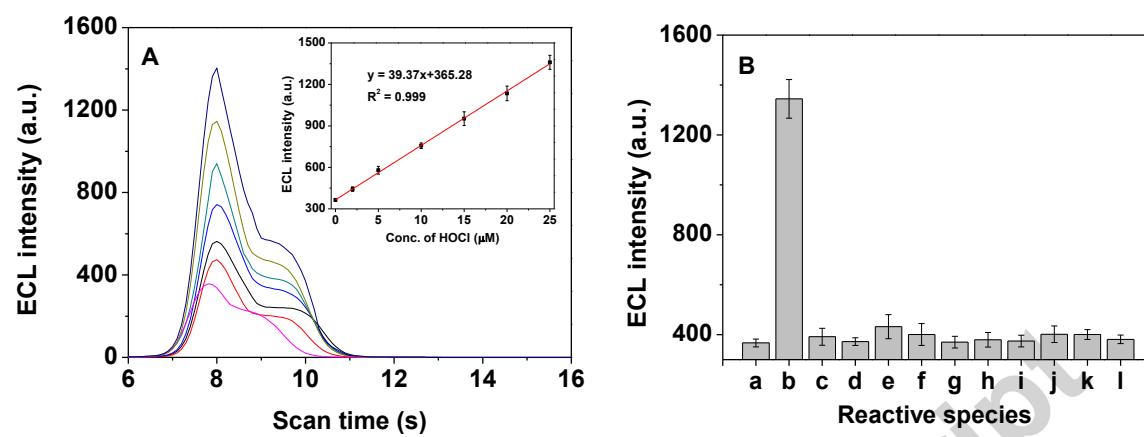
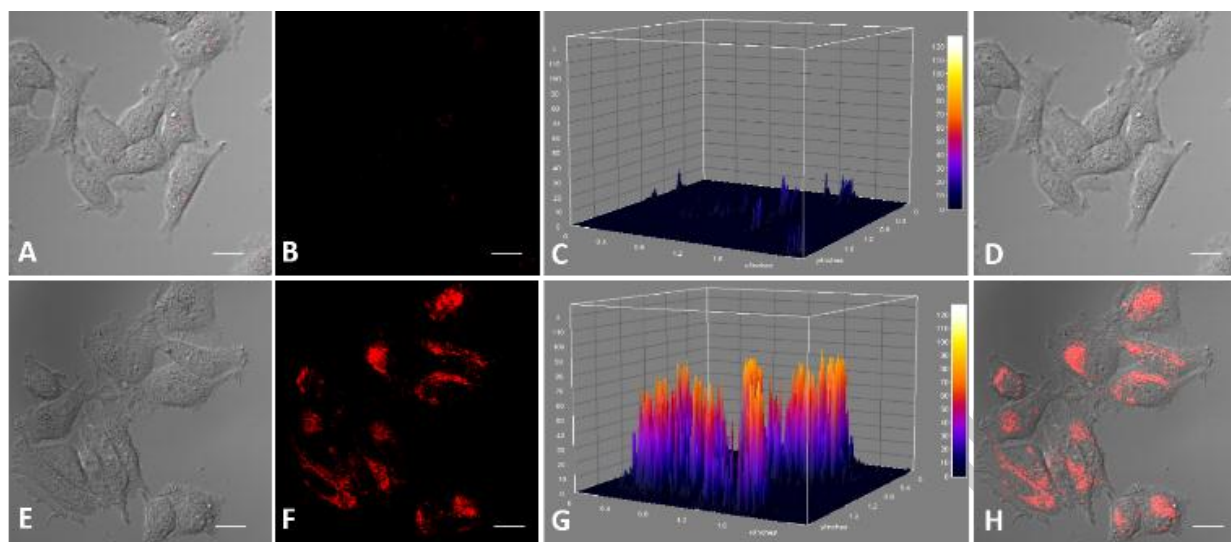
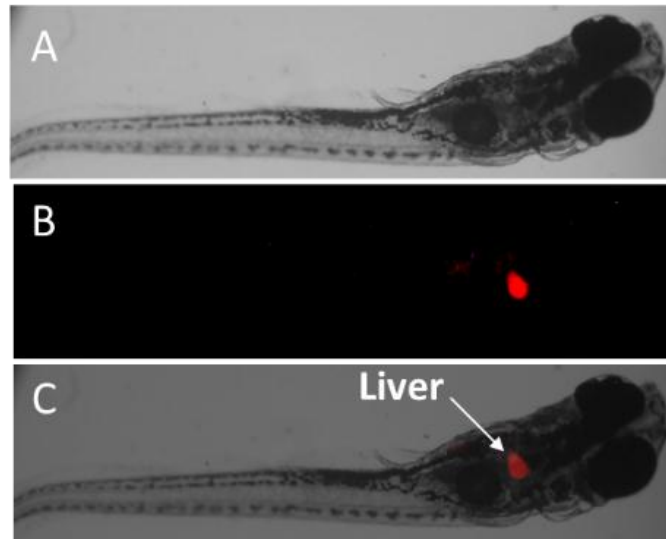


Fig. 3



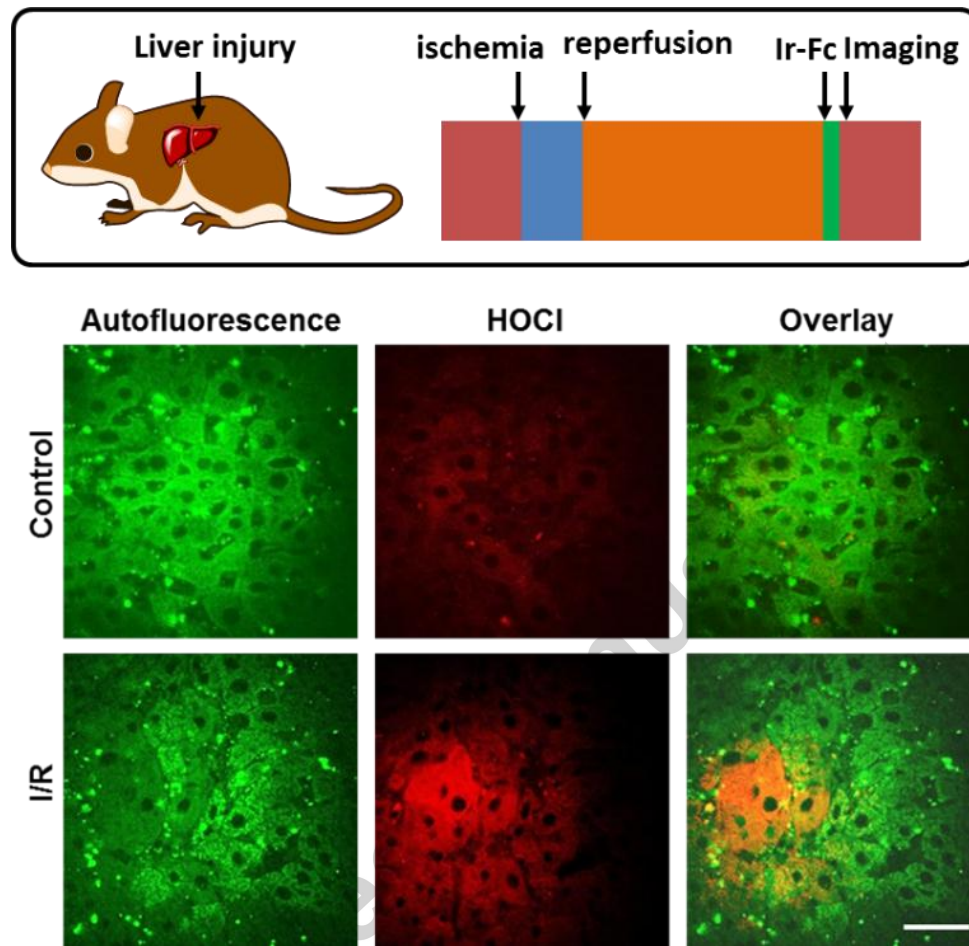
Accepted manuscript

Fig. 4



Accepted manuscript

Fig. 5.



Accepted manuscript